RSC Advances

ROYAL SOCIETY OF CHEMISTRY

www.rsc.org/advances

Cite this: DOI: 10.1039/c0xx00000x

www.rsc.org/xxxxxx

ARTICLE TYPE

Urchin-like Au-nanoparticles@Ag-nanohemisphere Arrays as Active SERS-substrates for Recognition of PCBs

Haibin Tang,[a] Guowen Meng,*[a,b] Qing Huang,[c] Chuhong Zhu,[a] Zhulin Huang,[a] Zhongbo Li,[a] Zhuo Zhang[a] and Yao Zhang[b]

Received (in XXX, XXX) Xth XXXXXXXXX 20XX, Accepted Xth XXXXXXXXX 20XX
DOI: 10.1039/b000000x

A simple fabrication route is developed for ordered urchin-like Au-nanoparticles decorated Ag-nanohemisphere nanodot arrays with highly active and reproducible surface-enhanced Raman scattering effect for rapid recognition of 4-chlorinated biphenyl.

Surface-enhanced Raman scattering (SERS) spectroscopy has been developed rapidly in chemical, environmental and biological sensing applications due to its high sensitivity, rapid response and fingerprint characteristics.[1-2] In order to fabricate effective SERS-substrates, various materials and structures have been tried in the past decades. Among them, noble metal nanoparticles (NPs) have drawn much attention because they can induce plenty of sub-10-nm gaps (so called "hot spots") between the NPs and thus induce enormous SERS effect.[3] However, it is difficult to achieve signal uniformity and reproducibility as the NPs are not uniformly distributed. Therefore, much effort has been devoted to the fabrication of uniformly distributed noble metal NP arrays to ensure the signal reproducibility, such as focused-ion-beam lithography,[4] electron-beam lithography,[5] and nanosphere-assisted lithography[6]. In contrast, the use of self-organized nanoporous anodic aluminum oxide (AAO) template as a direct fabrication route to metallic nanostructure arrays is an easy way and shows the advantage of long-range ordering, mechanical stability, good reproducibility and facile controllability of shape configurations.

In general, there are two routes for the AAO template-assisted fabrication of Ag NP (Ag-NP) arrays. (1) Ag is directly decorated,[7] or sputtered onto the top surface of the AAO template,[8-10] and the resultant small Ag-NPs are distributed only on the protrusions of the neighboring AAO-pore wall, so the density of the Ag-NPs is not high enough. (2) Ag-NPs arrays are achieved on a planar substrate with a ultrathin AAO template as mask,[11-12] but it is difficult to achieve sub-10-nm gaps between the neighboring Ag-NPs as the ultrathin AAO masks with sub-10-nm pore wall thickness are too brittle to manipulate. Additionally, it should be mentioned that the surface of the Ag-NPs achieved via the above two routes is smooth, which is not beneficial to high SERS-activity as rough metal surface could induce higher SERS-activity.[13-15] Then, Ag or Au hierarchical particles with rough surface, such as sea urchin-like,[15] flower-like,[13] meatball-like,[14] and star-like[16] morphologies, have been synthesized. Nevertheless, most of them are obtained through organic reduction routes using specific stabilizer or surfactant, which might bring signal interference in the subsequent SERS measurement. In addition, it is still a challenge to disperse these hierarchical particles uniformly on planar substrates to achieve SERS signal reproducibility.

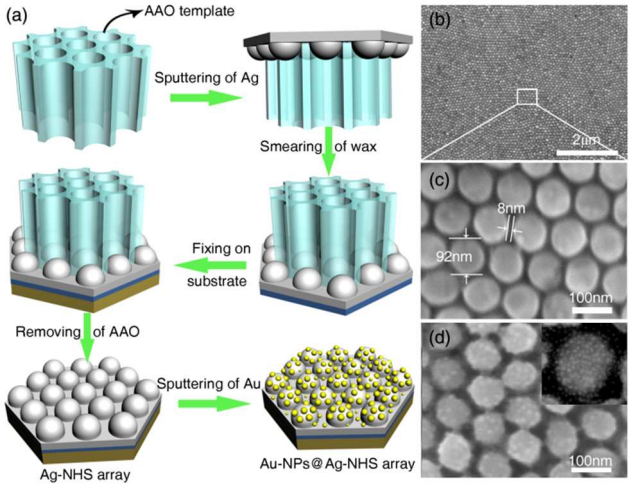

Fig.1 (a) The scheme of the fabrication route to urchin-like Au-NPs@Ag-NHS nanodot arrays. (b) SEM image and (c) a close-up view of the Ag-NHS arrays. (d) An enlarged view of the urchin-like Au-NPs@Ag-NHS arrays, the inset is the high-resolution SEM image.

Herein, we present a rational route to urchin-like Au-NPs decorated Ag-nanohemisphere (Ag-NHS) (denoted as Au-NPs@Ag-NHS) arrays as effective SERS-substrate, as shown schematically in Fig. 1(a). First, Ag is sputtered onto the top surface of highly ordered and hexagonally arranged nanoporous AAO template being heated up to 0.24 times of Ag melting point, and Ag aggregations occur and expand downwards the AAO-pores to form Ag-NHSs.[8] Then, wax and a Si wafer are attached to fix and support the Ag-NHS arrays before the removal of AAO template. Finally, small Au-NPs are sputtered onto the Ag-NHS surface to achieve three dimensional (3D) uniformly arranged urchin-like Au-NPs@Ag-NHS nanodot arrays.

As shown in the scanning electron microscopy (SEM) image of Fig. 1(b), large-scale uniform Ag-NHS arrays are achieved. An enlarged-view (Fig. 1(c)) displays that the Ag-NHSs are hexagonally arranged, with an average diameter of 92 nm and neighboring gap about 8 nm. The height of the Ag-NHS is about

65 nm, as shown in the side-view SEM image in Fig. S1 in ESI†. After top-sputtering Au onto the Ag-NHS arrays for 10 s, tens of small Au-NPs with a dimension of 5 ~ 10 nm are assembled onto the surface of each Ag-NHS, ultimately forming 3D hexagonally arranged and uniformly distributed urchin-like Au-NPs@Ag-NHS nanodot arrays, as shown in Fig. 1(d) and Fig. S2 in ESI† (for higher resolution).

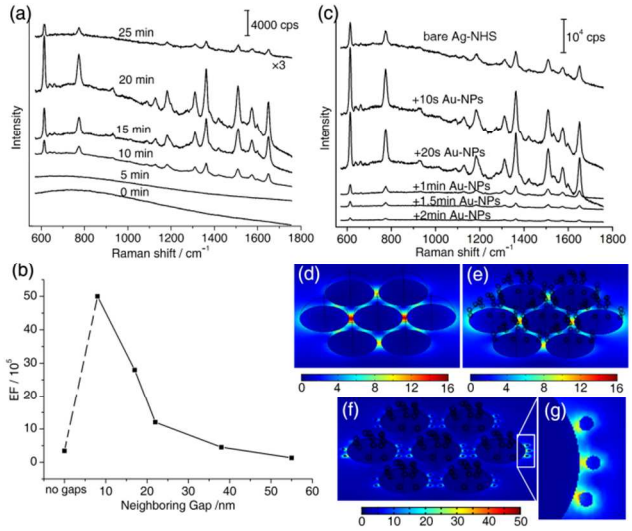

Fig.2 The SERS-sensitivity (a) and EF (b) evolution of the Ag-NHS arrays with the increase of AAO pore-widening duration (corresponding to the narrowing of neighboring gaps), (c) SERS-sensitivity evolution of the urchin-like Au-NPs@Ag-NHS arrays with the increase of Au-sputtering duration. The localized electrical field distribution for (d) the bare Ag-NHS arrays with 8-nm-gaps and (e) after decoration of Au-NPs, and (f) between the decorated Au-NPs and the Ag-NHSs. (g) An enlarged-view of (f). "cps" means counts per second.

As all the Ag-NHSs are formed inside the AAO pores, and replicate the uniform geometrical distribution and diameter of the nanopores, therefore the diameter of the Ag-NHSs and the neighboring gaps can be tailored by tuning the AAO pore-widening duration (Fig. S3 in ESI†), and the corresponding SERS-sensitivity evolution is manifested in Fig. 2(a) using 3×10^{-7} M R6G as probe molecules with an integration time of 1 s. When the pore-widening period is short (e.g., 5 min), the SERS-sensitivity is too low to distinguish the characteristic peaks of 3×10^{-7} M R6G. With the prolongation of pore-widening, the SERS-sensitivity of the substrate increases remarkably. When the pore-widening period prolongs to 20 min, the SERS-sensitivity is the highest. For a much longer pore-widening duration (25 min for example), the SERS-sensitivity decreases dramatically. This sensitivity evolution with the narrowing of the neighboring gaps of the Ag-NHS arrays can be explained by the electromagnetic enhancement mechanism as follows.[17-18] When the pores are widened for 0 or 5 min (Fig. S3 (a) and S3 (b)), the Ag-NHSs are not formed distinctly and the gaps between the neighboring Ag-NHs are very wide (55 nm and 38 nm, respectively). As a result, the plasmon coupling between the neighboring Ag-NHSs is not efficient and consequently the SERS-activity is low. With the pore-widening period for 10 or 15 min (Fig. S3 (c) and S3 (d)), the Ag-NHSs become distinct, and the neighboring gaps become narrower and narrower (22 nm and 17 nm, respectively), consequently the plasmon coupling becomes more efficient and the resultant SERS-activity is improved gradually. When the AAO-pores are widened for 20 min, as shown in Fig. 1(c), the neighboring gaps become as narrow as 8 nm, which can create highly efficient SERS "hot spots" and thus highest SERS-activity. With further prolongation of the pore-widening duration, 25 min for example, the Ag-NHSs become to bunch together and the neighboring gaps disappear (Fig. S3(e)), i.e. the "hot spots" disappear, leading to the dramatic decrease of SERS-activity. The SERS-sensitivity evolution law is also demonstrated by the enhancement factor (EF) dependence with the neighboring gaps, as shown in Fig. 2(b). With the narrowing of the neighboring gaps, the EF is improved, and for the 8 nm gaps the EF is about 0.5×10^7 (the detailed estimation is shown in Part S4 in ESI†). Once the gaps disappear, the EF decreases to 3.4×10^5.

Fig. 2(b) reveals the SERS-sensitivity evolution of the urchin-like Au-NPs@Ag-NHS hybrid nanodot arrays achieved via Au-sputtering for different durations onto the Ag-NHS arrays with neighboring gaps of 8 nm. Once the Au-NPs are sputtered onto the surface of the Ag-NHSs for 10 s, the SERS-activity is improved in comparison with that from the bare Ag-NHS arrays. However, with longer Au-sputtering, the SERS-activity decreases dramatically, especially for longer than 20 s. These phenomena can be explained by the morphology evolution (especially the gaps of neighboring Ag-NHs) with Au-sputtering for 20 s, 1 min, 1.5 min and 2 min, as shown in Fig. S5 in ESI†. A short Au-sputtering (10 s) can only create small Au-NPs on the surface of Ag-NHs and does not cram the neighboring gaps. Therefore both the plasmon coupling between the neighboring Ag-NHSs and that between the Ag-NHS and the decorated Au-NPs will occur efficiently and consequently contribute to the SERS-activity improvement. It should also be mentioned that after the Au-NPs decoration the surface of Ag-NHSs becomes rougher, which could induce higher SERS-activity.[13-15] If the Au-sputtering is further prolongated, the number and size of the decorated Au-NPs will dramatically grow up. Bigger Au-NPs will shape around the Ag-NHSs to occupy the neighboring gaps, resulting in the disappearance of "hot spots" between the neighboring Ag-NHSs and consequently the decrease of SERS-activity. Additionally, since the SERS enhancement of Au is about 2 orders lower than that of Ag, the more the Au content with elongation of the Au-sputtering, the more the dramatic decrease of SERS-activity.[19]

These SERS-sensitivity evolutions are also demonstrated by theoretical calculation with finite-difference time-domain (FDTD) analysis. Fig. S6 and Fig. 2(c) show the localized electrical field distribution between the gaps (17 nm and 8 nm) of the neighboring bare Ag-NHSs fabricated by using AAO templates with pore-widening for 15 and 20 min, respectively. When the neighboring gaps are 17 nm, the local electric field is enhanced by about 10.0 times. However, once the gaps are narrowed to about 8 nm, the local electric field is enhanced by about 15.7 times, clearly indicating the improvement of the localized field with the narrowing of the gaps between the neighboring Ag-NHSs, which is concordant with the experimental results. Further, once the Au-NPs are decorated onto the surface of the Ag-NHSs, the field enhancement occurs not only between the neighboring Ag-NHSs (shown in Fig. 2(e)), but also between the decorated Au-NPs and the Ag-NHSs (shown in Fig. 2(f) and (g)). The localized field between the neighboring

Ag-NHSs is enhanced by about 10 times, which slightly decreases after the decoration of Au-NPs. However, the localized field between the Ag-NHS and decorated Au-NPs is enhanced by up to 49 times, much larger than that between the bare Ag-NHSs (15.7). Considering the EF, to the first approximation, can be expressed by the fourth power of the ratio of the total electric field to the incident excitation field,[20] the maximum EF of the urchin-like Au-NPs@Ag-NHS nanodot arrays could reach to 0.58×10^7.

The SERS enhancement effect and signal uniformity of the urchin-like nanodot arrays with 10 s Au-sputtering onto the surface of Ag-NHSs with 8 nm neighboring gaps are manifested in Fig. 3. As shown in Fig. 3(a), the intensity of the spectral characteristic peaks of R6G decreases with the concentration decrease from 10^{-9} M to 10^{-14} M. The sensitivity of the as-prepared substrates is so high that R6G molecules even at a low

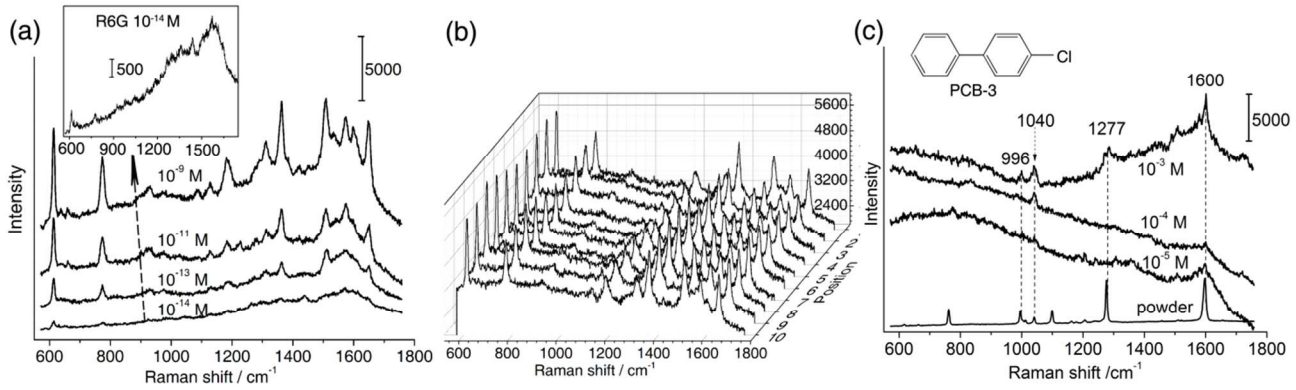

Fig.3 The SERS spectra of (a) R6G with different concentrations with an integration time of 10 s, (b) 10^{-8} M R6G collected from 10 random spots on the substrate with an integration time of 2 s. (c) The SERS spectra of PCB-3 with concentrations from 10^{-3} M to 10^{-5} M with an integration time of 30 s, and the Raman spectrum of pure PCB-3 powder (the bottom curve) with an integration time of 10 s.

concentration of 10^{-14} M can be clearly identified. Additionally, to further manifest the SERS-activity of the urchin-like Au-NPs@Ag-NHS arrays, the EF is estimated to be 1.23×10^7 (shown in detail in Part S7 in ESI†), which has the same order of magnitude high as that of the FDTD simulation, and is higher than that of the bare Ag-NHS arrays. On the other hand, the good signal uniformity of the urchin-like Au-NPs@Ag-NHS arrays is tested, as shown in Fig. 3(b). All the Raman spectra of R6G, obtained from 10 random spots on the same piece of substrate, have approximative intensity for each characteristic band, which can be attributed to the uniform morphology of the Ag-NHS arrays in large scale.

Finally, the urchin-like Au-NPs@Ag-NHS nanodot arrays are used as SERS-substrates for the identification of PCB-3, one congener of PCBs (one class of persistent organic pollutants defined in Stockholm Convention).[21-22] The Raman spectra of PCB-3 collected from the optimal substrates with concentrations of 10^{-3} M, 10^{-4} M and 10^{-5} M are shown in Fig. 3c. It can be seen that the Raman intensity of PCB-3 characteristic peaks falls with the concentration decrease of PCB-3 solution. Even at a low concentration of 10^{-5} M, the Raman characteristic bands of PCB-3 can be clearly identified, and the bands at 996 and 1040 cm^{-1} are attributed to ring trigonal breathing modes, while the bands at 1277 and 1600 cm^{-1} are assigned to the C-C bridge stretching mode and aromatic ring stretching mode, respectively.[23-24]

In summary, uniform 3D urchin-like Au-NPs@Ag-NHS nanodot arrays have been fabricated via AAO template-assisted approach, and show excellent SERS performance. The Ag-NHSs are formed in the ordered nanopores of the AAO template with desired pore-wall thickness, so that the Ag-NHSs are uniformly arranged in large scale with sub-10-nm neighboring gaps. Furthermore, small Au-NPs are decorated onto the surface of the Ag-NHSs, forming urchin-like Au-NPs@Ag-NHS nanodot arrays, and the SERS-sensitivity is further improved owing to the enhanced surface-roughness. The resultant substrates demonstrate high SERS-sensitivity to 10^{-14} M R6G and 10^{-5} M PCB-3. Therefore, the urchin-like Au-NPs@Ag-NHS nanodot arrays have great potentials as effective SERS-substrates for rapid detection and monitoring of trace PCBs.

This work was financially supported by the National Key Basic Research Program of China (2013CB934304), the National Natural Science Foundation of China (Grants No. 11274312, 21303211).

Notes and references

[a] *Key Laboratory of Materials Physics, and Anhui Key Laboratory of Nanomaterials and Nanostructures, Institute of Solid State Physics, Chinese Academy of Sciences, Hefei, Anhui 230031, P. R. China. E-mail: gwmeng@issp.ac.cn; Fax: +86 551 65591434; Tel: +86 551 65592749*
[b] *University of Science and Technology of China, Hefei, Anhui 230026, P. R. China.*
[c] *Institute of Technical Biology and Agriculture Engineering, Hefei Institutes of Physical Sciences, Chinese Academy of Sciences, Hefei, Anhui 230031, P. R. China.*

† Electronic Supplementary Information (ESI) available: Experimental section, additional Fig.s and EF estimation. See DOI: 10.1039/b000000x/

1 M. P. Cecchini, A. Wiener, V. A. Turek, H. Chon, S. Lee, A. P. Ivanov, D. W. McComb, J. Choo, T. Albrecht, S. A. Maier and J. B. Edel, *Nano Lett.*, 2013, **13**, 4602-4609.
2 S. Shanmukh, L. Jones, J. Driskell, Y. Zhao, R. Dluhy and R. a. Tripp, *Nano Lett.*, 2006, **6**, 2630-2636.
3 N. J. Borys, E. Shafran and J. M. Lupton, *Sci. Rep.*, 2013, **3**.
4 A. G. Brolo, E. Arctander, R. Gordon, B. Leathem and K. L. Kavanagh, *Nano Lett.*, 2004, **4**, 2015-2018.
5 Q. Yu, P. Guan, D. Qin, G. Golden and P. M. Wallace, *Nano Lett.*, 2008, **8**, 1923-1928.

6 S. H. Lee, K. C. Bantz, N. C. Lindquist, S.-H. Oh and C. L. Haynes, *Langmuir*, 2009, **25**, 13685-13693.
7 P. Pinkhasova, H. Chen, M. W. G. M. Verhoeven, S. Sukhishvili and H. Du, *RSC Advances*, 2013, **3**, 17954.
8 J. Wang, L. Huang, L. Yuan, L. Zhao, X. Feng, W. Zhang, L. Zhai and J. Zhu, *Appl. Surf. Sci.*, 2012, **258**, 3519-3523.
9 T. Qiu, W. Zhang, X. Lang, Y. Zhou, T. Cui and P. K. Chu, *Small*, 2009, **5**, 2333-2337.
10 T. Qiu, F. Kong, X. Yu, W. Zhang, X. Lang and P. K. Chu, *Appl. Phys. Lett.*, 2009, **95**, 213104.
11 H. F. Liu, E. S. Lim, P. K. H. Tung and N. Xiang, *Thin Solid Films*, 2011, **519**, 3050-3054.
12 Y. Takahashi and T. Tatsuma, *Nanoscale*, 2010, **2**, 1494-1499.
13 H. Liang, Z. Li, W. Wang, Y. Wu and H. Xu, *Adv. Mater.*, 2009, **21**, 4614-4618.
14 H. Wang and N. J. Halas, *Adv. Mater.*, 2008, **20**, 820-825.
15 J. Fang, S. Du, S. Lebedkin, Z. Li, R. Kruk, M. Kappes and H. Hahn, *Nano Lett.*, 2010, **10**, 5006-5013.
16 M. J. Mulvihill, X. Y. Ling, J. Henzie and P. Yang, *J. Am. Chem. Soc.*, 2010, **132**, 268–274.
17 H. Im, K. C. Bantz, N. C. Lindquist, C. L. Haynes and S. H. Oh, *Nano Lett.*, 2010, **10**, 2231-2236.
18 S. J. Lee, Z. Guan, H. Xu and M. Moskovits, *J. Phys. Chem. C*, 2007, **111**, 17985-17988.
19 M. Erol, Y. Han, S. K. Stanley, C. M. Stafford, H. Du and S. Sukhishvili, *J. Am. Chem. Soc.*, 2009, **131**, 7480.
20 K. Kneipp, Y. Wang, H. Kneipp, L. T. Perelman, I. Itzkan, R. Dasari and M. S. Feld, *Phys. Rev. Lett.*, 1997, **78**, 1667-1670.
21 J. L. Daniels, M. P. Longnecker, M. A. Klebanoff, K. A. Gray, J. W. Brock, H. B. Zhou, Z. Chen and L. L. Needham, *Am. J. Epidemiol.*, 2003, **157**, 485–492.
22 T. Z. Zheng, T. R. Holford, J. Tessari, S. T. Mayne, P. H. Owens, B. Ward, D. Carter, P. Boyle, R. Dubrow, S. Archibeque-Engle and S. H. Zahm, *Am. J. Epidemiol.*, 2000, **152**, 50–58.
23 Z. L. Huang, G. W. Meng, Q. Huang, B. Chen, C. H. Zhu and Z. Zhang, *J. Raman Spectrosc.*, 2013, **44**, 240-246.
24 Q. Zhou, Y. Yang, J. Ni, Z. Li and Z. Zhang, *Nano Research*, 2010, **3**, 423-428.

Graphical Abstract

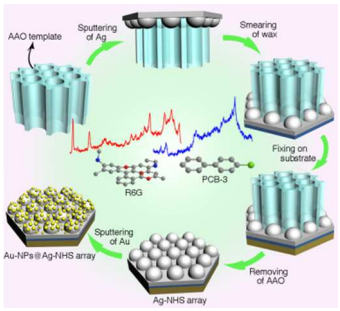

Short abstract for graphical abstract:

Large-scale ordered urchin-like Au-nanoparticles decorated Ag-nanohemisphere nanodot arrays show highly active surface-enhanced Raman scattering effect for rapid recognition of PCB-3.